



HAL
open science

Molecular beam study of CO oxidation on Pd clusters supported on alumina: effect of cluster size

Georges Sitja, Claude Henry

► **To cite this version:**

Georges Sitja, Claude Henry. Molecular beam study of CO oxidation on Pd clusters supported on alumina: effect of cluster size. *Physical Chemistry Chemical Physics*, 2024, 26 (21), pp.15338-15343. 10.1039/d4cp01030b . hal-04731920

HAL Id: hal-04731920

<https://hal.science/hal-04731920v1>

Submitted on 11 Oct 2024

HAL is a multi-disciplinary open access archive for the deposit and dissemination of scientific research documents, whether they are published or not. The documents may come from teaching and research institutions in France or abroad, or from public or private research centers.

L'archive ouverte pluridisciplinaire **HAL**, est destinée au dépôt et à la diffusion de documents scientifiques de niveau recherche, publiés ou non, émanant des établissements d'enseignement et de recherche français ou étrangers, des laboratoires publics ou privés.

Molecular beam study of CO oxidation on Pd clusters supported on alumina: effect of cluster size

Georges Sitja and Claude R. Henry

CNRS, CINaM, Aix-Marseille Université

F-13288 Marseille, France

Abstract

The activity in CO oxidation of regular arrays of Pd clusters, in the size range 5 – 180 atoms, supported on alumina has been studied by a molecular beam method. The Pd clusters are grown on a nanostructured ultrathin alumina film on Ni₃Al (111) providing a hexagonal array of clusters with a narrow size distribution. The steady state turnover frequency (TOF) is measured as a function of the mean cluster size. The TOF increases with size. Below about 20 atoms, the TOF increases rapidly and for larger clusters it grows slowly and reaches at 180 atoms a value close to those obtained on bulk single crystals. The size effect is explained by the smaller activity of Pd atoms in contact with the alumina support.

1. Introduction

CO oxidation on metals from Pt group is one of the most studied reaction [1]. On single crystals (Pt, Pd) Ertl and co-workers have evidenced that the reaction mechanism is of Langmuir-Hinshelwood type by using molecular beam methods [2]. The reaction is considered as structure insensitive because the catalytic activity, for given reaction parameters, is almost independent of the surface structure [2]. Following a Boudart statement, a structure insensitive reaction should not depend on the metal particle size [3]. Later, Boudart and Poppa have studied the CO oxidation reaction, at low pressure, on Pd nanoparticles grown under UHV on α -alumina single crystals [4]. The size of the Pd particles was measured by TEM. They showed that in the CO rich-regime (low temperature) the catalytic activity per surface atom and per second (TOF: Turnover frequency) is independent of particle size while in the O-rich regime (high temperature) the TOF is constant for large sizes but increases when particle sizes decreases from 4 to 1.5 nm. This fact, in contradiction with the expectations for a structure insensitive reaction, was later explained by an effect of reverse-spillover of CO on the alumina support [5, 6]. The reverse-spillover effect corresponds to the capture by metal clusters of CO physisorbed diffusing on the oxide support. It depends on the size and on the surface density of clusters. A detailed account of

this effect can be found in a recent review [7]. A molecular beam study of CO oxidation on Pd clusters (2.8, 6.8 and 13 nm), epitaxially grown on MgO (100), has shown similar results: an increase of the TOF when particle size decreases [8]. The reverse spillover fitted perfectly the TOF vs temperature curve for the larger particles while for smaller ones, only a reasonably good agreement was obtained. This small discrepancy was attributed to an intrinsic size effect due the presence of different facets and surface defects while the reverse spillover was defined as an extrinsic size effect [9]. By the same molecular beam technique, a decrease of the TOF has been observed on 1.8 nm Pd particles on alumina ultrathin film compared to 5.5 nm particles [10]. All these surface science studies of CO oxidation on supported model catalysts were limited by a rather large size distribution (size dispersion at least 25% of the mean size).

In order to reduce the size dispersion, metal clusters can be grown epitaxially on a template constituted by a nanostructured substrate leading to regular arrays of clusters [7]. For model catalysis studies, a particularly interesting support is an ultrathin alumina film obtained by high temperature oxidation of a Ni₃Al (111) surface [11]. On these arrays of clusters, the size dispersion is close to $1/\sqrt{N}$, N being the mean number of atoms in the clusters [7]. Another advantage of these arrays is that the effect of the reverse spillover on the reaction kinetics can be exactly calculated [7]. The CO oxidation reaction has been studied on Pd clusters with a size of 181 ± 13 atoms by a molecular beam method. After correction of the reverse-spillover effect the steady state TOF was found equal to those measured on Pd (111) [12]. A more recent study by the same method has shown that the TOF for clusters from 2 to 5 atoms was constant and that single atoms are not active [13].

However, to know the activity of a cluster with a precise number of atoms the only way is to prepare clusters in the gas phase and to select a particular size by a mass filter, before deposition on the substrate at low kinetic energy [14]. Several groups have studied catalytic oxidation of CO of size-selected deposited Pd clusters between 1-30 atoms [14-18]. However, in most of these studies the reactivity was studied by thermal programmed reaction (TPR) of pre-adsorbed of CO and O₂ molecules at low temperature. This method does not provide a steady state activity that could be compared with measurements on supported nanoparticles or single crystals. Meanwhile, steady state activity measurements have been obtained either by pulsed valves [16] or by capillary tubes coming close to the sample surface [18]. For the first study on Pd clusters of 8, 13 and 30 atoms supported on MgO (100) thin films, the activity per the total number of atoms in the clusters shows a maximum of the TOF for 13 atoms [16]. However, as the 30 atoms clusters are expected to be tridimensional only surface atoms are active then the real TOF must be larger. In the second study, the steady state activity per atom was measured for clusters of 5, 20 and 25 atoms deposited on alumina films and found to increase with cluster size [18]. Another way to have a very narrow size distribution of nanoparticles is

to use colloidal synthesis giving size dispersion below 6%. Murray and coworkers used this method for Pd nanoparticles (diameters of 2.5, 3.8 and 6 nm) supported on alumina and ceria powders [19]. On alumina, no size effect was observed. On ceria, the TOF increased with decreasing size. In this last case, the size effect is explained by a larger activity at the periphery of the nanoparticles via a Mars-van Krevelen reaction mechanism [20] that does not occur for non-reducible supports like alumina.

In this paper we measure by a molecular beam method the steady state activity of CO oxidation on regular arrays of Pd clusters, with a low size dispersion, grown on alumina on Ni₃Al (111) surface. The mean size of the clusters is varied from 5 to 180 atoms. We see that for small clusters (5 to 20 atoms), the TOF increases rapidly with size and for larger cluster it increases slowly towards the value measured for extended Pd surfaces. The observed variations are discussed in term of intrinsic size effects due to interface atoms and low coordinated atoms and extrinsic size effect due to reverse-spillover of reactants.

2. Experimental section

2.1 Sample preparation

The alumina ultrathin films are prepared following the method of C. Becker [21]. Ni₃Al(111) surfaces are prepared several cycles of argon sputtering and annealing at 1100 K. The temperature of the sample is precisely measured by a thermocouple in contact with the Ni₃Al single crystal and by an optical pyrometer. The alumina ultrathin film is obtained by high temperature (1000K) oxidation of the Ni₃Al surface under pure oxygen (5×10^{-8} mbar, total exposure of 45 L). The quality of the alumina film is *in situ* checked by low electron energy diffraction (LEED). Pd clusters are epitaxially grown, by deposition at 373 K, of a flux of Pd atoms ($2.3 \pm 0.03 \times 10^{12}$ atoms/s.cm²) issued from a water cooled Knudsen cell. The Pd flux is *in situ* measured before each deposition by a quartz microbalance. During Pd deposition, the pressure in the UHV chamber remains in the 10⁻¹⁰ mbar range. The Pd clusters grow exclusively on the 'dot' structure of the alumina film forming a hexagonal array of clusters with a Poisson distribution (the size dispersion $\Delta N/N = 1/\sqrt{N}$ %, N being the mean number of atoms in the clusters). The density of clusters is constant and equal to the density of nodes of the 'dot' structure ($n_s = 6.5 \times 10^{12}$ cm⁻²) [11]. The quality and the reproducibility of the organization of the clusters has been checked *in situ* by STM and GISAXS (grazing incidence X-ray scattering) in previous studies [11, 22].

2.2 Reactivity measurements

The reactivity of the Pd clusters is studied at constant temperature with a background pressure of isotopically labeled oxygen (¹⁸O₂) and a CO molecular beam. The CO beam is produced by supersonic expansion and is collimated in order that all CO molecules impinge only the sample surface. The intensity of the CO beam ($J_{CO} = 2 \times 10^{13}$ cm⁻²s⁻¹, equivalent pressure: $P_{CO} = 6.8 \times 10^{-8}$ mbar) is modulated

by a programmable shutter. The background pressure in the vacuum chamber increases to 5×10^{-10} mbar when the CO beam is on. The intensity of the flux of molecules leaving the substrate (CO_2 and unreacted CO) are measured by a quadrupole mass spectrometer working in a pulse-counting mode. Before introducing $^{18}\text{O}_2$ in the chamber the intensity of the flux of CO leaving the sample is measured (at $T > 473$ K the adsorption of CO on the Pd clusters is fully reversible then the desorbing flux is equal to the impinging flux). Generally, we divide the CO_2 flux (V_{CO_2}) by the CO impinging flux in order to be insensitive to a change of the mass spectrometer sensitivity; this ratio is called the global reaction probability (RPg). To measure the CO_2 resulting from the CO oxidation reaction we detect the mass 46 corresponding to $^{12}\text{C}^{16}\text{O}^{18}\text{O}$ produced by the Langmuir-Hinshelwood mechanism. We have shown previously that no CO_2 is produced via the Mars van Krevelen mechanism [13].

3. Experimental results

3.1 Effect of substrate temperature

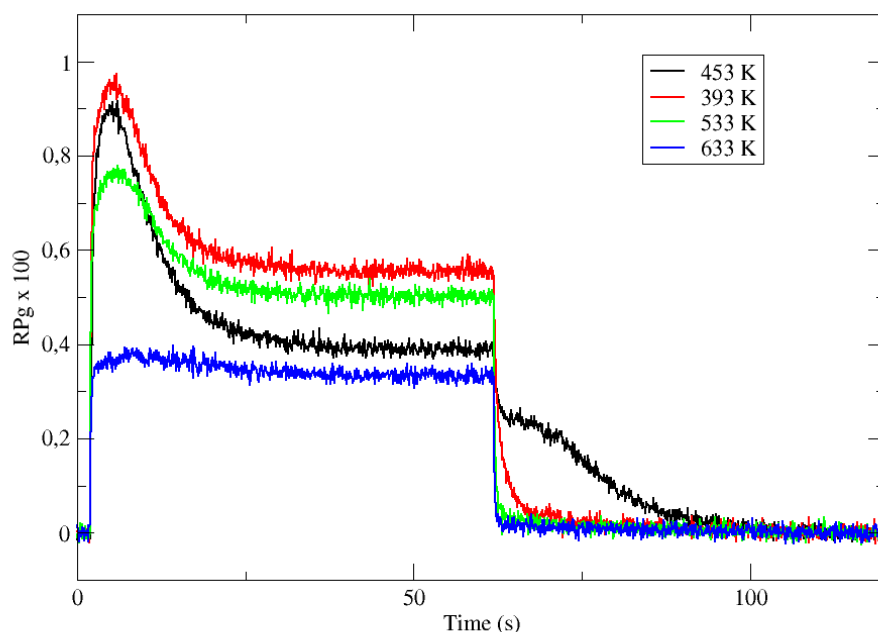


Figure 1: Time evolution of the CO_2 production in response of a molecular beam pulse of CO in a background of oxygen (1.1×10^{-8} mbar) on clusters of 80 ± 9 atoms at various temperatures.

Figure 1 displays the global reaction probability ($\text{RPg} = V_{\text{CO}_2}/J_{\text{CO}}$) of CO_2 production from the sample surface for an isotropic pressure of oxygen $P_{\text{O}_2} = 1 \times 10^{-8}$ mbar and a pulse of CO, as a function of time and for different substrate temperatures measured for 80 ± 9 atoms. It can be seen that after a

transient period when the CO beam is turned on and a steady state is installed at about 30 seconds. The variations of the steady state value as a function of substrate temperature are plotted on Figure 2.

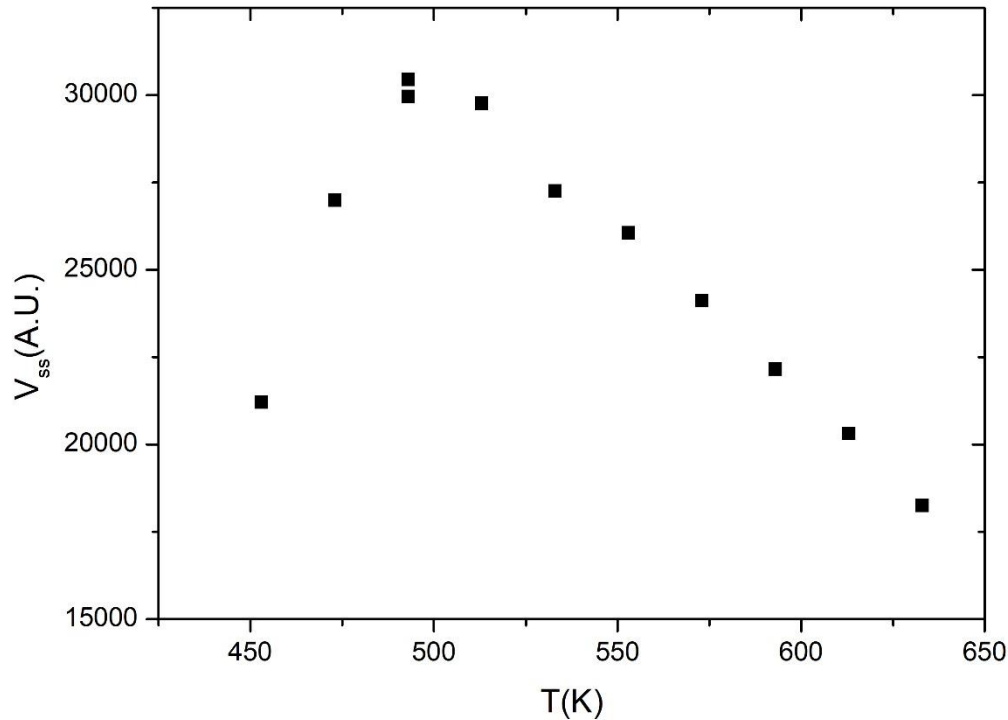


Figure 2: Steady state CO₂ production as a function of temperature on 80 ± 9 Pd clusters.

When temperature increases the steady state production of CO₂ increases rapidly and reach a maximum near 500 K, then it slowly decreases. This is a typical evolution already observed on Pd extended surfaces [2] and on supported nanoparticles [4, 8, 12] or clusters [18]. At low temperature, the CO coverage is large and impedes the dissociative adsorption of oxygen leading to low reaction rates. When temperature increases the CO coverage decreases and the reaction rate grows. This is the 'CO-rich' regime. At high temperature, the oxygen coverage is large and close to saturation but the CO coverage is low and decreases rapidly because of fast CO desorption explaining why the CO₂ production drops; this is the 'O-rich' regime. The CO₂ transient peak, observed on figure 1 occurs in the CO rich regime. When the CO beam is on, the O-coverage (θ_o) is close saturation and CO coverage (θ_{CO}) increases rapidly with time then the θ_o/θ_{CO} ratio decreases down to the optimal value for the reaction at the maximum of the peak then it starts to decrease towards the steady state value. At high temperature in the O-rich regime θ_o/θ_{CO} at steady is always larger than the optimal value then the transient peak is no longer observed. On figure 2 at 453 K when the CO beam is closed, a CO₂ production is still observed for about 30 s. This second peak of CO₂ is due to a high CO coverage

inhibiting oxygen adsorption at steady state, then when the CO beam is turned off, oxygen coverage increases rapidly increasing the reaction rate until the consumption of all adsorbed CO. The second peak of CO₂ production has been already observed in CO-rich regime on Pd nanoparticles [8, 9, 23, 24, 25]. It is not only due to the inhibition of oxygen adsorption at high CO coverage but it also occurs when defects are present on the Pd nanoparticles [9, 23, 25].

3.2 Effect of oxygen pressure

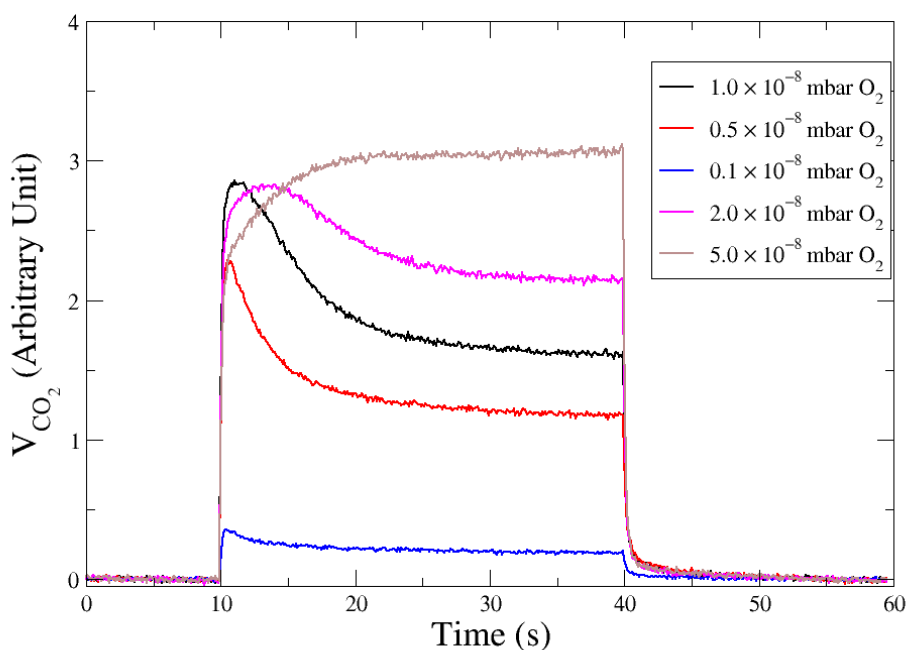


Figure 3: Time evolution of the CO₂ production in response of a molecular beam pulse of CO in a background of oxygen with various pressures, on clusters of 180±13 atoms at 533K.

Figure 3 displays CO₂ pulses obtained on Pd clusters containing 180 ± 13 atoms at 533K and for various oxygen pressures. We can see that a CO₂ transient peak is present at lower oxygen pressures and not for the largest oxygen pressures. Like previously, it corresponds to cases where $P_{O_2}/P_{CO} < 0.5$ (corresponding to the stoichiometry of the reaction) for which the steady state coverage of CO is large. Figure 4 shows that the steady state production of CO₂ increases with oxygen pressure, as expected in the CO-rich regime.

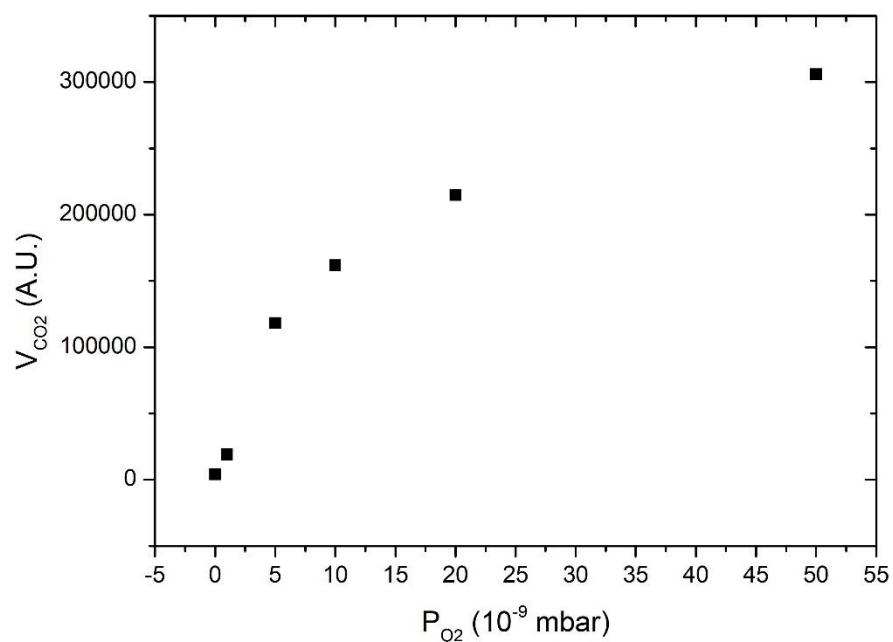


Figure 4: Steady state production of CO₂ as a function of oxygen pressure at 533K on clusters of 180±13 atoms.

3.3 Size effect

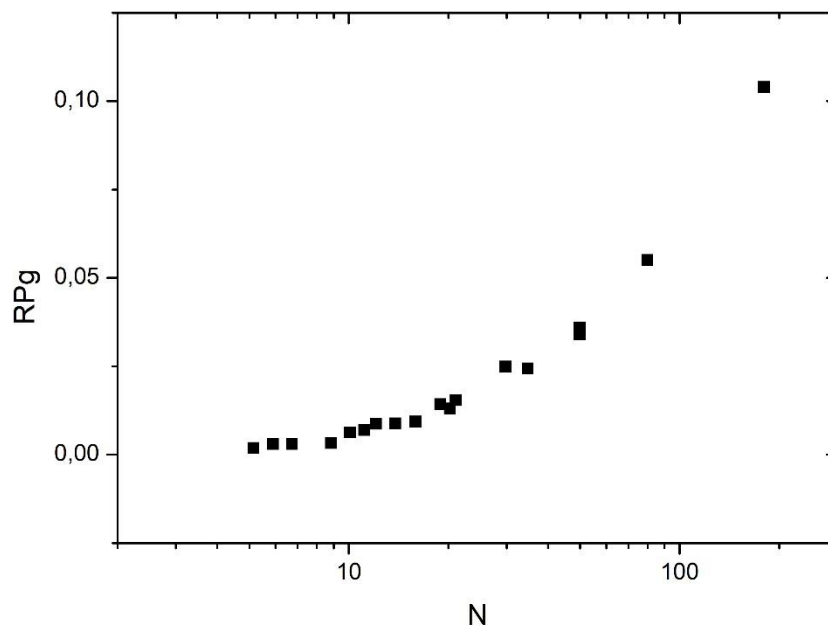


Figure 5: Activity in CO oxidation (RP_g) at 533K plotted as function of the mean number of atoms in the clusters. ($P_{O_2}/P_{CO} = 0.19$).

In Figure 5 the global reaction probability is plotted as a function of the mean cluster size (N). Below about 10 atoms, the activity (RP_g) evolves slowly but for larger sizes it increases more rapidly. We can also calculate the activity per cluster (A_{clu}) that is equal to $(RP_g J_{CO})/n_s$. In fact it is equal to $3.077 RP_g$. The activity per cluster increases non-linearly with cluster size. This behavior was expected because, when the size of the clusters increases the number of exposed atoms per cluster increases. In order to correct this effect we calculate the activity per deposited atoms (A_{at}) by dividing A_{clu} by N. On figure 6 we can see that, on average, A_{at} increases rapidly with cluster size below about 20 atoms then A_{at} slowly decreases. In fact, at small sizes, fluctuations of the reactivity are visible. These fluctuations are due several reasons. Firstly, there is a distribution of the cluster size even it is small. It is known from studies of purely size selected clusters [14] that the activity depends on the exact number of atoms in the cluster [14]. Secondly, for a given number of atoms a cluster can have different shapes (fluxionality) that correspond to different catalytic activities. However despite these fluctuations there is, on the means, a net increase of the activity when the mean size (N) increases.

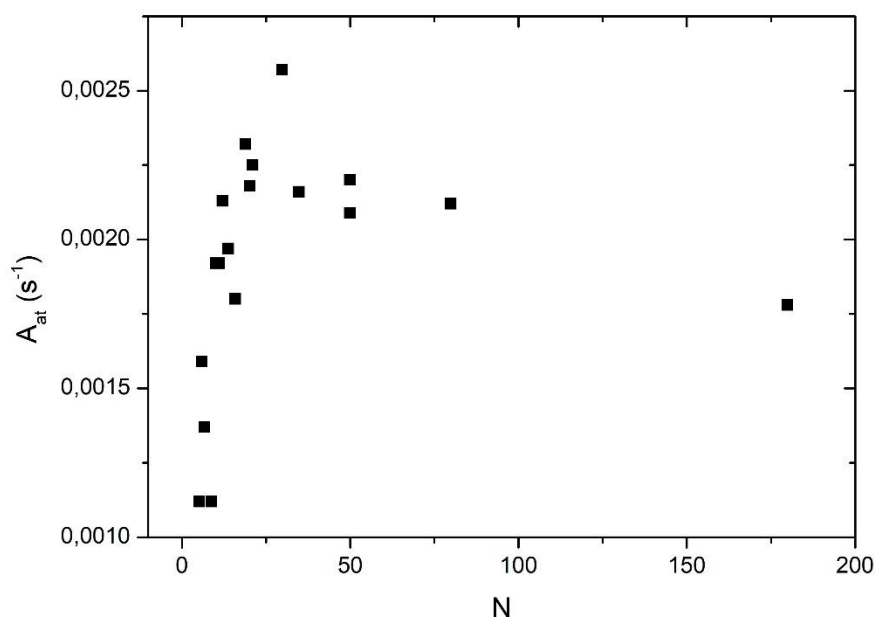


Figure 6: Activity per atom at 533K as function of the number of atoms (N) in the clusters.

At this point, we have to remind that the larger clusters (80 and 180 atoms) have a 3D-shape and that the smallest ones are 2D allowing all the atoms to be active, contrary to larger clusters. In fact, we have to calculate the activity per surface atoms that is the TOF. However, to calculate the TOF we have to know the exact shape of the clusters. In a previous study, we concluded that the clusters smaller than five atoms are 2D [13]. From STM studies, we concluded that clusters containing at least 35 atoms are 3D [11]. Assuming the shape of a truncated sphere, we found a contact angle of 92° meaning an almost

hemispherical shape [11]. For size-selected Pt clusters deposited on alumina ultrathin films on NiAl(110) the group of Watanabe has found, from STM studies, that the transition between monolayer and bilayer clusters occurs around 20 atoms and the growth of the third layer appears around 30 atoms [26]. In order to derive the TOF we consider that clusters from 5 to 19 atoms are 2D, the 19-atoms cluster being a regular hexagon. We also assume that from 20 to 31 atoms the second layer grows and that a third layer is present between 32 and 37 atoms. We call this model of cluster 'layer model'.

Taking into account the model for the cluster shape it is possible to calculate the number of surface atoms (N_s) and then the TOF that is equal to $A_{at} \times (N/N_s)$. For Larger clusters, we will use the hemispherical model. The number of surface atoms divided by the total number of atoms is $N_s/N = 3N_0v_0/R$. N_0 is the number of atoms per unit area (we take $1.53 \times 10^{15} \text{ cm}^{-2}$ corresponding to a Pd (111) surface) and v_0 the Pd atomic volume ($1.47 \times 10^{-23} \text{ cm}^3$). The cluster radius $R = (3v_0/2\pi)^{1/3} \cdot N^{1/3}$. Figure 7 displays the TOF values calculated from the two models (layer model and hemisphere model) the two models overlap for the point at $N = 35$ atoms. The layer model shows a rapid increase (more or less linear) of the TOF when the number of atoms increases from 5 to about 30 atoms. The hemispherical model shows a slow evolution toward a saturation around 180 atoms. It is clear that the two model cannot be extrapolated over 35 atoms for layer model and below 35 atoms for the hemispherical model.

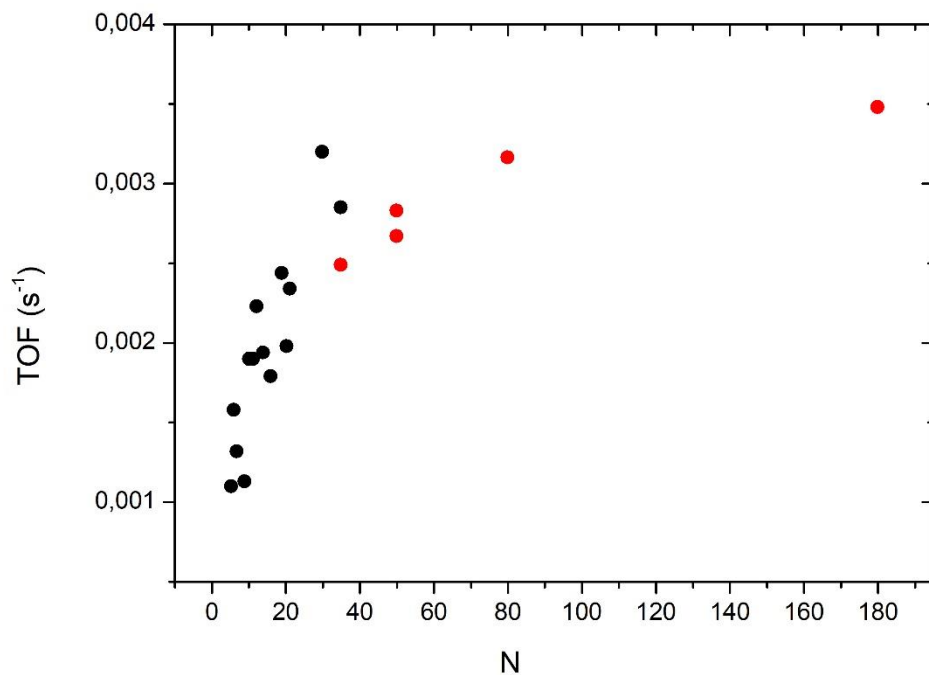


Figure 7: TOF at 533K as a function of the mean number of atoms in the clusters. The number of surface atoms is calculated by the layer model (black points) or by a hemisphere model (red points) for the cluster shape.

4. Discussion

4.1 Size effect for small sizes: role of interface atoms (N = 5 – 30 atoms)

Figure 7 shows two different behaviors for large and small clusters. For small clusters (below 30 atoms), the TOF decreases rapidly when cluster size decreases. We can expect that the lowering of activity is related to the interaction of interface Pd atoms with the substrate that decreases their activity. However, if we consider that all interface atoms are less active than the other atoms one would expect a constant (low) TOF between 5 to 19 atoms (following the layer model) but it is not the case. We have also to take into account for the coordination of the interface atoms with neighboring Pd atoms, higher is this coordination number lower is the decrease of activity by the interaction with the substrate. Watanabe et al [26] considered such effect in the case of CO oxidation on 2D Pt clusters. Without theoretical calculation, it is difficult to take precisely account of the effect of the coordination. Following this model, for clusters larger than 20 atoms only interfacial atoms at the periphery of the clusters would have a reduced activity. When the size further increases, the proportion of these periphery atoms decreasing rapidly, the effect of reduced activity of periphery atoms would be less important

4.2 Size effect for large clusters (N=35-180)

For large clusters the TOF increases slowly and tends to saturate at N=180. Previously, we have measured the TOF for N= 181± 13 atoms and shown that after correction of the reverse-spillover effect the TOF was nearly the same as for a Pd(111) extended surface [12]. In order to know if the increase of the TOF for large cluster is only due to the reverse-spillover effect we have calculated this effect (See Supplementary Information). After correction of the reverse-spillover, the TOF for clusters between 35 and 180 atoms would increase by a factor 1.6 proving that there is still an intrinsic size effect in this range of size. When cluster size decreases below 35 atoms the effect of the reverse-spillover increases then this effect cannot explain the strong increase observed, for small clusters, when the mean size increases between 5 and 35 atoms.

5. Conclusion

The steady state activity in CO oxidation has been measured on arrays of Pd clusters with a mean size varying from 5 to 180 atoms and supported on an ultrathin alumina film on Ni₃Al (111). Below about 20 atoms, on the average the TOF increases rapidly with the mean cluster size. For clusters larger than 35 atoms, the TOF increases slowly towards the bulk value which is already reached at 180 atoms. For a mean size between 5 to 180 atoms, the TOF increases by a factor 3. This size effect can be decomposed in an intrinsic size effect and an extrinsic size effect. The intrinsic size effect is mainly due to a smaller activity of the atoms in contact with the support. The extrinsic size effect is due to the reverse spillover of CO that increases the flux of CO arriving on the clusters; it depends on cluster size, on the distance between clusters and on the substrate temperature.

REFERENCES

- [1] H.J. Freund, G. Mejer, M. Scheffler, R. Schlögl, M. Wolf; CO oxidation as a prototypical reaction for heterogeneous processes. *Angew. Chem. Int. Ed.* 50(2011)10064-10094
- [2] T. Engel, G. Ertl; Catalytic oxidation on platinum metals. *Adv. Catal.* 28(1979)1
- [3] M. Boudart, *Adv. Catal. Relat. Subj.* 20(1969)153
- [4] S. Ladas, H. Poppa and M. Boudart; The adsorption and Catalytic oxidation of carbon monoxide on evaporated palladium particles. *Surf. Sci.* 102(1981)151-171
- [5] F. Rumpf, H. Poppa and M. Boudart; Oxidation of carbon monoxide on palladium: role of the alumina support. *Langmuir* 4(1988)722-728
- [6] C.R. Henry, On the effect of the diffusion of carbon monoxide on the substrate during CO oxidation on supported palladium clusters. *Surf. Sci.*(1989)519-526
- [7] C.R. Henry ; 'Perspectives' 2D-Arrays of nanoparticles as model catalysts. *Catal. Lett.* 145(2015)731-749
- [8] C. Becker, C.R. Henry, Cluster size dependent kinetics for the oxidation of CO on a Pd/MgO(100) model catalyst. *Surf. Sci.* 352-354(1996)457-462
- [9] C.R. Henry, Reaction Dynamics on Supported Metal Clusters in 'The Chemical Physics of Solid Surfaces, Vol. 11: Surface Dynamics' Eds. D.P. Woodruff, Elsevier (2003) Ch. 9 pp. 247-290
- [10] I. Meusel, J. Hoffman, J. Hartmann, J. Libuda, H.J. Freund; *J.Phys. Chem. B* 105(2001)3567: Size dependent reaction kinetics on supported model catalysts: A molecular beam/IRAS study of the CO oxidation on alumina supported Pd particles.
- [11] M. Marsault, G. Sitja, C.R. Henry ; Regular arrays of Pd and PdAu clusters on ultrathin alumina films for reactivity studies. *Phys.Chem. Chem. Phys.* 16(2014)26458-26466
- [12] G. Sitja, C.R. Henry; Molecular beam study of the oxidation of carbon monoxide on a regular array of Palladium clusters on alumina. *J. Phys. Chem. C* 121(2017)10706
- [13] G. Sitja, C.R. Henry; Activity of Pd_n (n=1-5) clusters on alumina film on Ni₃Al (111) for CO oxidation: a molecular beam study. *J. Phys. Chem. C*.125 (2021)13247-13253
- [14] T.M. Bernhardt, U. Heiz, U. Landman; Chemical and catalytic properties of size-selected free and supported clusters in 'Nanocatalysis', U. Heiz, U. Landman Eds, Springer-Verlag Berlin, 2007

- [15] U. Heiz, A. Sanchez, S. Abbet, W.D. Schneider; Tuning the oxidation of carbon monoxide using nanoassembled model catalysts. *Chem. Phys.* 262(2000)189
- [16] C. Harding, S. Kunz, V. Habibpour, V. Teslenko, M. Arenz, U. Heiz; Dual pulsed-beam controlled mole fraction studies of the catalytic oxidation of CO over supported Pd nanocatalysts. *J. Catal.* 255(2008)234-240
- [17] W.E. Kaden, T. Wu, W.A. Kunkel, S.L. Anderson; Electronic structure controls reactivity of size selected Pd clusters adsorbed on TiO₂ surfaces. *Science* 326(2009)826-829
- [18] M.D. Kane, F. S. Roberts, S.L. Anderson; Mass-selected supported cluster catalysts: Size effects on CO oxidation activity, electronic structure, and thermal stability of Pd_n/alumina (n ≤ 30) model catalysts. *Int. J. Mass Spectrom.* 370(2014)1-15
- [19] M. Cargnello, V.V.T. Doan-Nguyen, T.R. Gordon, R.E. Diaz, E.A. Stach, R.J. Gorte, P. Fornasiero, C.B. Murray; *Science* 341(2013)771-773: Control of metal-support interface. Role of ceria catalyst. *Science* 341(2013)771-773
- [20] G. Spezzati, A.G. Benavidez, A.T. DeLaRiva, Y. Su, J.P. Hofmann, S. Asahina, E.J. Olivier, J.H. Neethling, J.T. Miller, A.K. Datye, E.J.M. Hensen; CO oxidation by Pd supported on CeO₂(100) and CeO₂(111) facets. *Appl. Catal. B Environmental* 243(2019)36-46.
- [21] A. Rosenhahn, J. Schneider, C. Becker, K. Wandelt; Oxidation of Ni₃Al(111) at 600, 800, and 1050 K investigated by scanning tunneling microscopy. *J. Vac. Sci. Technol. A* 18(2000)1923-1927
- [22] G. Sitja, S. Le Moal, M. Marsault, G. Hamm, F. Leroy, C.R. Henry; *Nano Letters*, 13(2013) 1977-1982: Transition from molecule to solid state: reactivity of supported metal clusters. *Nano Letters*, 13(2013) 1977-1982
- [23] L. Piccolo, C. Becker and C.R. Henry; Kinetic modelling of the CO oxidation reaction on supported metal clusters. *Euro. Phys. J. D* 9(1999)415-419
- [24] J. Libuda, I. Meusel, J. Hoffmann, J. Hartmann, L. Piccolo, C.R. Henry and H.J. Freund; The CO Oxidation Kinetics on Supported Pd Model Catalysts: A molecular Beam / In-situ IRAS study. *J. Chem. Phys.* 114(2001)4669-4684
- [25] J. Hoffmann, I. Meusel, J. Hartmann, J. Libuda, H.J. Freund; Reaction kinetics on heterogeneous model catalysts: The CO oxidation on alumina-supported Pd particles. ; *J. Catal.* 204(2001)378
- [26] A. Beniya, S. Higashi, N. Ohba, R. Jinnouchi, H. Hirata, Y. Watanabe; CO oxidation activity of non-reducible oxide-supported mass-selected few-atom Pt single-clusters. *Nat. Commun.* 11(2020)1888

Supplementary Information

Calculation of reverse-spillover effect